2021

Numerical Simulation of the Heat Transfer in a Refrigerated Trailer Equipped with Eutectic Plates for Frozen Food Delivery

Jihyuk Jeong
Université de Sherbrooke, jihyuk.jeong@usherbrooke.ca

Alla Eddine Benchikh Le Hocine
Université de Sherbrooke

Sergio Croquer
Université de Sherbrooke

Sébastien Poncet
Université de Sherbrooke

Jocelyn Bonjour
CETHIL, INSA Lyon, Lyon, France

See next page for additional authors

Numerical Simulation of the Heat Transfer in a Refrigerated Trailer Equipped with Eutectic Plates for Frozen Food Delivery

Jihyuk JEONG[1,2*], Alla Eddine BENCHIKH LE HOCINE[1], Sergio CROQUER[1], Sébastien PONCET[1], Jocelyn BONJOUR[2], Benoit MICHEL[2]

[1]Mechanical Engineering Department, Université de Sherbrooke, Sherbrooke, Québec, Canada
Alla.Eddine.Benchikh.Lehocine@USherbrooke.ca; Sergio.Croquer.Perez@USherbrooke.ca; Sebastien.Poncet@USherbrooke.ca

[2]CETHIL, INSA Lyon, Lyon, France
jocelyn.bonjour@insa-lyon.fr; benoit.michel@insa-lyon.fr

*Corresponding author: Jihyuk.Jeong@USherbrooke.ca

ABSTRACT

The present work reports the Computational Fluid Dynamics simulation and analysis of the heat transfer inside a refrigerated truck trailer equipped with three eutectic plates and fans. The numerical model solves the conjugated heat transfer inside the trailer in 2D using the $k-\omega$ Shear Stress Transport (SST) turbulence model. It has been already favorably validated against the numerical and experimental data of Lafaye de Micheaux el al. (2015) by Croquer et al. (2019). These simulations are used to improve the configuration of the refrigeration system with the eutectic plates as well as to investigate the feasibility of the eutectic plates for the transport of frozen food products under different operating loads and transport temperature requirements. Three eutectic plates having an optimal inter-plate distance of 6 cm to maximize the air flow between the plates (Croquer et al., 2019) are either placed in series on the roof of the trailer or vertically at its back. For both configurations, fans are blowing the air from the eutectic plates to the inside of the trailer and modeled by adding a source term into the momentum equations. During the door opening period, the configuration with the plates placed on the roof of the trailer without the cargo has noticeably lower area-averaged temperature inside the trailer than the configuration with the plates placed on the back of the trailer due to the presence of the circulation zones and the cold plates located near the doorway. However, introduction of the cargo into the simulations eliminates the formation of the circulation zones that prevents the infiltration of the atmospheric air. Also, the configuration with the plates placed on the roof of the trailer allows the atmospheric air to infiltrate earlier, therefore resulting in an overall higher temperature observed in the cargo.

1. INTRODUCTION

Around 2% of the total greenhouse gas emissions in developed countries are due to food transport, including motive power and refrigeration (Tassou et al., 2009). For temperature-controlled transport vehicles, legislations are in place to provide common standards and to provide certification (UN Economic Commission for Europe, 2018). Road transport vehicles employ different types of refrigeration units depending mainly on the size of the vehicle and its load. For medium to large vehicles, refrigeration units powered by a self-contained diesel engine are primarily used. To guarantee -20°C within the trailer, the fuel consumption is typically up to 4 liters per hour for a semi-truck trailer with an inside volume of 78.79 m^3 (Tassou et al., 2009). Refrigeration systems solely based on the eutectic plates have been developed and used in prototype vehicles in the recent years to overcome such fuel consumption (Bonaventure et al., 2020; Croquer et al., 2019). Eutectic system typically consists of tubes, beams or plates filled with a phase of change materials to store energy and produce a cooling effect. During the typical delivery cycle, eutectic plates absorb heat infiltrated into the trailer as latent heat and ensure the maintenance of the desired temperature inside the trailer for about 8 hours (Croquer et al., 2019). Furthermore, the eutectic plates are charged at night when the electricity is off peak load. However, heat losses through frequent door opening are a major concern, especially in humid climates. Frequent door opening account for the majority of the heat infiltration during the typical delivery cycle as well as inducing condensation and the formation of ice along the plates. Thick condensed layers of frost and ice formed along

the plates interfere with the heat transfer between the eutectic plates and the surrounding air, effectively nullifying the effects of the eutectic plates.

The heat and mass transfer phenomena inside a refrigerated chamber have been well studied and received significantly more attention (Azzouz et al., 1993; Foster et al., 2003; Hoang et al., 2000). However, there is a limited number of studies investigating the heat and mass transfer phenomena inside a truck trailer with frequent door openings. Tso et al. (2002) investigated the influence of the air, fan and plastic strip air curtains. The authors demonstrated that the deployment of an air curtain can lead to energy savings of 40% to 11% compared to cases without an air curtain and with a plastic strip curtain respectively. Lafaye de Micheaux et al. (2015) numerically and experimentally investigated the velocity and temperature distributions inside of the truck trailer with different door opening parameters. Croquer et al. (2019) fully modeled a truck trailer equipped with the eutectic plates by CFD. The model was validated against the experimental and numerical data of Lafaye de Micheaux et al. (2015) to model the heat transfer inside a truck trailer operated by the eutectic system. The $k-\omega$SST turbulence model with the production terms representing buoyancy contributions to the turbulent field has been employed by Croquer et al. (2019) and demonstrated a slight improvement compared to the predictions of the $k-\varepsilon$model of Lafaye de Micheaux et al. (2015).

The main objective of the present study is to extend the former works of Croquer et al. (2019) and Bonaventure et al. (2020) using the same validated CFD model to optimize the configuration of the refrigeration system with the eutectic plates in terms of trailer temperature, cargo temperature, and infiltration heat load. As Lafaye de Micheaux et al. (2015) and Croquer et al. (2019) demonstrated that the 3D effects do not significantly influence the velocity or temperature distributions at the midplane of the doorway, a 2D approach is adopted in this study. Eutectic refrigeration systems with three plates placed in series on the roof or at the back of the trailer are investigated. To simulate the infiltration of the outside warm air during the door opening period, a method of implementing a wind tunnel outside of the trailer is employed. Steady state results are obtained and applied as an initial condition for the transient simulations to observe the interaction between the existing developed flow inside the trailer and the outside air. Furthermore, the same simulations are repeated for different loadings of frozen meat inside the trailer to investigate the influence of the cargo.

2. NUMERICAL MODELING

The model presented in Croquer et al. (2019) has been adapted in 2D with a detailed unstructured mesh as well as minor boundary, geometric and parametric changes to investigate the flow.

2.1. Geometrical modeling

For all the system configurations, the truck trailer is 7.13 m long and 2.616 m high. The plates are 1.76 m long and 0.054 m wide, containing a frozen eutectic mixture that acts as the cooling source. During the normal operating condition and typical short time day delivery cycle, the fusion inside the plates keep their surfaces at a constant temperature of 244 K for about 8 hours (Croquer et al., 2019). Two configurations are primarily investigated: three eutectic plates in parallel at the back (Configuration A) and three eutectic plates in series located at the roof of the trailer (Configuration B) as seen in Figure 1. The inter plate spacing is 6 cm. This value has been identified to be the optimal value to maximize the airflow between the plates (Croquer et al., 2019). For all configurations, the distance between the plates and the walls and the separating wall are all set to be 6 cm.

Four fans are mounted above the plates for Configuration A and to the left of the plates in Configuration B to maintain the air circulation between the plates and the trailer. Two air circulation modes can be employed: blowing mode and suction mode. For the blowing mode, air is blown out from the plate region to the trailer and for the suction mode, air is sucked into the plate region. Fans are modeled via the addition of a source term, $\rho_{air}U_{fan}$, in the momentum equations with the characteristic value of $U_{fan} = 8.4$m.s^{-1} to match the existing fans (mass flow rate of 0.04 kg.s^{-1}, Reynolds number $Re = 1.6 \times 10^6$ based on the fan diameter). The blowing mode was found to be the optimal operating mode by Croquer et al. (2019) in terms of the trailer temperature. Nevertheless, it remains of interest to investigate the interaction between the developed flow structure inside the trailer and the incoming outside warm air, both for the suction and blowing operating modes.

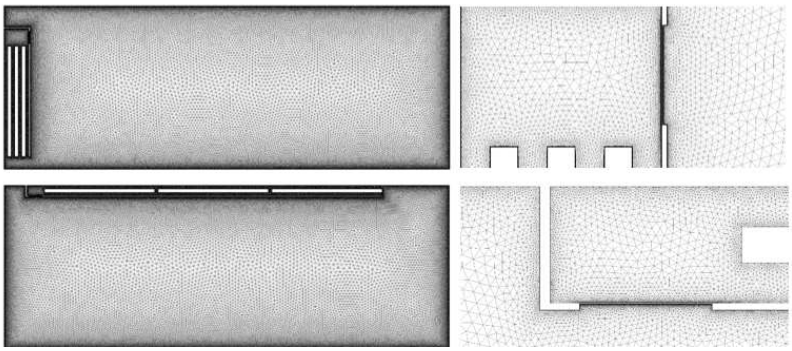

Figure 1: Overview of the mesh for Configuration A (top) and Configuration B (bot) with the fan and the plates region focused on the right.

2.2. Numerical method

All calculations are performed using the finite-volume software CFX ANSYS v19. The Unsteady Reynolds Averaged Navier-Stokes equations (URANS) as well as the conservation of mass and total energy are solved to model the flow and heat transfer. Buoyancy driven flows with temperature differences greater than 20 K are expected. Dry air is assumed to be an ideal gas with variable density but constant transport properties. The Boussineq model is used to model for the density change. Turbulent effects are incorporated by using the $k-\omega$ SST turbulence model with the production terms representing the buoyancy contributions to the turbulent field. Second-order high resolution and second order backward-Euler schemes with implicit time-stepping are used for, respectively, the spatial and temporal discretization. A Rhie-Chow fourth order algorithm is applied to treat the pressure-velocity coupling.

2.3. Numerical parameters

Unstructured meshes composed of triangular elements are generated by Centaur for the spatial discretization of the 2D domain as shown in Figure 1. A minimum of 10 prismatic layers are added close to the walls with a growth ratio set to 1.1 and the thickness of the layers are set to ensure $y^+ < 1$ to impose a low-Reynolds number implementation of the automatic near wall treatment in CFX. The thickness of the first prismatic layer is approximately 1.2×10^{-5} m from the solid walls. The mesh grid is composed of 964 220 and 958 946 nodes for Configurations A and B, respectively, and provides grid-independent solutions.

For transient simulations, an adaptive time-step approach is adopted to ensure a smooth time convergence. The time step remains between 5×10^{-3}s and 1×10^{-3} s for all simulations. At each time step, the discretized URANS equations are solved using an inner loop with convergence criteria for mass, momentum and energy residuals RMS under 10^{-4}. From the parametric study, it has been identified that 3 to 5 target inner-loop iterations with convergence criteria of 10^{-4} results in a reasonable compromise between time and accuracy. Simulations are performed using 40 CPU nodes with 30GB RAM (Compute Canada, Béluga and Graham clusters). As a reference, the closed configuration in steady state converges approximately after 4 hours.

For the steady state calculations, the heat transfer through the walls is implicitly specified by an imposed external overall heat transfer coefficient $h = 0.4$W.m^{-2}. K^{-1} corresponding to a heavily insulated equipment (Bonaventure et al., 2020; Economic commission for Europe, 2018) with an outside atmospheric temperature of 293 K to model thermal resistance outside the trailer computational domain. The steady state calculations are initialized with constant pressure of 101 325 Pa, initial temperature of 253 K and a zero-velocity field inside the trailer. For the transient simulations, instantaneous door opening is assumed at $t = 0$ s and the fans are turned off. A wind tunnel with the dimension of 31 m long and 5.43m high is included to simulate the interaction between the air inside the trailer and the atmospheric air. The trailer is placed 9.99 m away from the wind tunnel wall, with the opposite side wall being an opening boundary condition, and 0.335 m above the ground. To allow for the heat transfer between the air inside the trailer and the air inside the wind tunnel through the walls, the thermal contact resistance of 1.84 m^2.K.W^{-1} based on typical refrigerated container insulation layers is used (Croquer et al., 2019). Initial parameters of the wind tunnel are fixed to be 293 K and 0 m.s^{-1} at $t = 0$s. Whereas the initial parameters for the trailer are taken from the results of the steady-state simulations. A general-connection interface is set at the opening doorway, through which the air can freely flow in any direction.

3. RESULTS AND DISCUSSION

Steady-state calculations are initially performed for the two configurations with the plates located at the back and the roof of the trailer. The aforementioned configurations are compared without and with a given cargo load. Afterwards, results obtained from the steady state simulations are imposed as the initial values inside the trailer before the door opening for the transient calculations to investigate the interaction between the developed fluid flow inside the trailer with the outside air.

3.1. Steady State Results

Configurations A and B without loading are compared for the steady state conditions. Figure 2 displays temperature and velocity contours inside the trailer. As shown in Table 1, it seems that regardless of the configuration, the counterclockwise flow that takes place inside the trailer results in an overall lower area-averaged temperature and in a higher velocity inside the trailer. Area-averaged velocity excluding the plates region being 15.7% and 29.1% higher than their clockwise counterparts for Configurations A and B, respectively. The area-averaged temperatures excluding the plate region only differ by 0.5 K from the maximum value obtained by Configuration A – suction mode of 245.6 K and the minimum value obtained by Configuration A – blowing mode of 245.1 K.

All the steady state results exhibit a similar flow pattern: i) main flow from the plate regions circulating along the trailer with near zero velocity zone near the center of the trailer, ii) the presence of weaker secondary circulation zones at each corner of the trailer. The maximum temperatures inside the trailer are observed in these corners.

Table 1: Temperature and velocity results obtained from the steady state simulations

Configuration	Maximum temperature (K)	Area-averaged temperature (K)	Area-averaged velocity ($m.s^{-1}$)
A – blowing	254.5	245.1	3.64
A – suction	252.1	245.6	4.21
B – blowing	253.5	245.4	4.30
B – suction	254.0	245.2	3.33

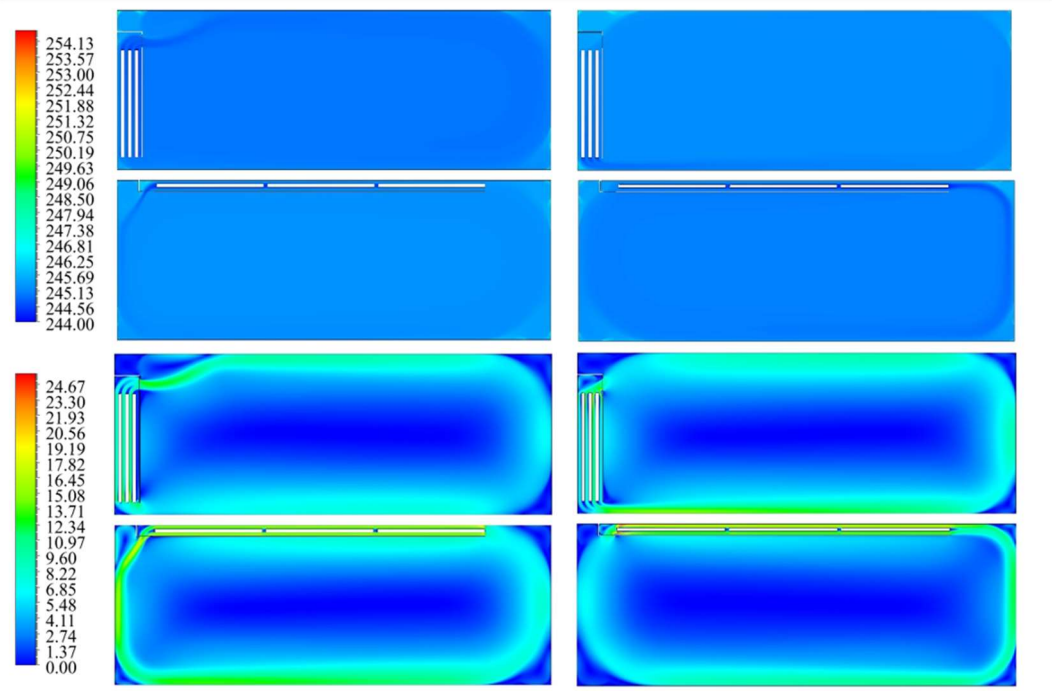

Figure 2: Temperature (K) and velocity ($m.s^{-1}$) contours of Configuration A blowing (top-left) and suction (top-right) and Configuration B blowing (bot-left) and suction (bot-right)

There are few distinctions that can be observed between each configuration:

For Configuration A – blowing mode, from the velocity contour, it is apparent that there is no flow present between the first plate and the separating wall, effectively reducing the influence of the plate. For Configuration B, all the plates are fully utilized.

For Configuration B, gravity plays a role in either reinforcing or weakening the strength of the flow. For the blowing mode, velocity of the flow downwards from the fan towards the bottom of the trailer is reinforced by gravity, therefore achieving the highest area-averaged velocity out of all the configurations. For the suction mode, as the flow is dragged from the bottom of the trailer to the plates, gravity weakens the flow, therefore resulting in the weakest area-averaged velocity. Similar conclusions can be obtained for the velocity field of Configuration A – suction mode being stronger than the blowing mode, but it is not as significant as seen from Configuration B.

3.2. Transient Results

The infiltration rate is defined as the volume flow rate of the air infiltrating into the trailer and the heat load is defined as the amount of heat exchange occurring through the entire doorway. The Infiltration rate ($\dot{V}$) and the heat load ($\dot{Q}$) across the doorway are calculated as follows:

$$\dot{V} = \iint_{P} u_n \, dA_{infiltration} \tag{1}$$

$$\dot{Q} = \iint u_n \frac{}{R_{specific} T} c_{da}(T - 273) dA_{door} \tag{2}$$

One defines u_n the velocity normal to the doorway with the positive direction towards the trailer, P the pressure, $R_{specific}$ =287.058 J.kg^{-1}.K^{-1} the specific gas constant of dry air and c_{da} =1006 J.kg^{-1}.°C^{-1} its specific heat. In Equation (2), a reference temperature of 273 K was chosen for the reference state of the enthalpies. To obtain the infiltration rate and heat load across the entire doorway, the obtained 2D values were scaled to that of 2.5 m in width as in Lafaye de Micheaux et al. (2015) and Croquer et al. (2019).

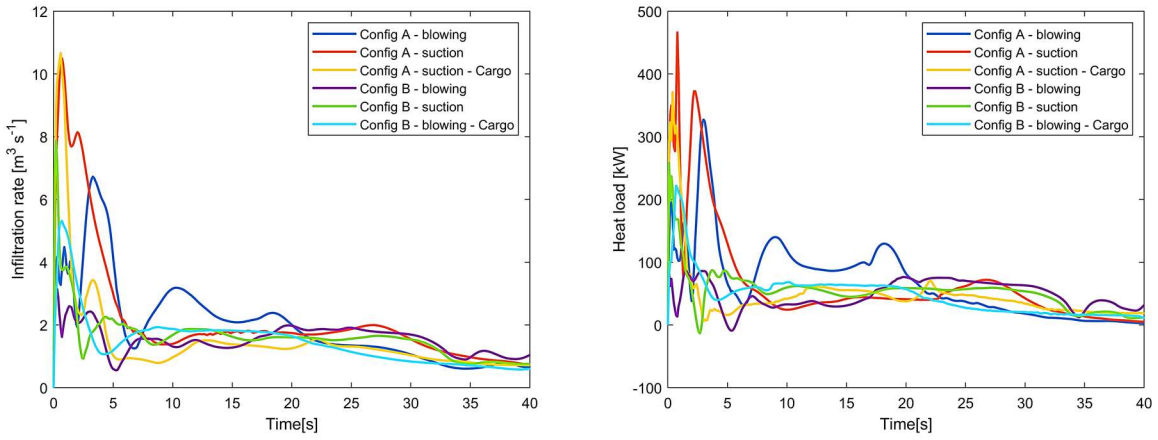

Figure 3: Temporal evolution of the a) infiltration rate (left) and b) heat load (right) through the door

The renewal time is defined as the time required by the internal air to be completely renewed (Lafaye de Micheaux et al., 2015). However, it should be noted that the simulation under investigation in this paper considers the existence of a pre-existing flow before the door opening. Therefore, the infiltration rate does not directly correspond to the amount of pure atmospheric air entering into the trailer. Especially in the first few seconds, the mixed temperature air created by the interaction between the cold strong velocity pre-existing flow and the hot atmospheric air can be the main source of infiltration. Moreover, exfiltration of mixed or atmospheric air can temporarily lead to a negative heat load induced through the doorway.

Table 2: Infiltration data obtained from the transient simulations without cargo

Configuration	Renewal Time (s)	Peak infiltration rate ($m^3.s^{-1}$)	Peak infiltration time (s)
A – blowing	14.5	6.7	3.3
A – suction	13.0	10.5	0.7
B – blowing	27.7	3.1	0.3
B – suction	24.5	7.9	0.2

However, it is apparent from Figure 3 that for the majority of the time, the heat load directly corresponds to the infiltration rate. Therefore, the infiltration rate and the renewal time are used as parameters to determine the performance of the configurations and the operating modes.

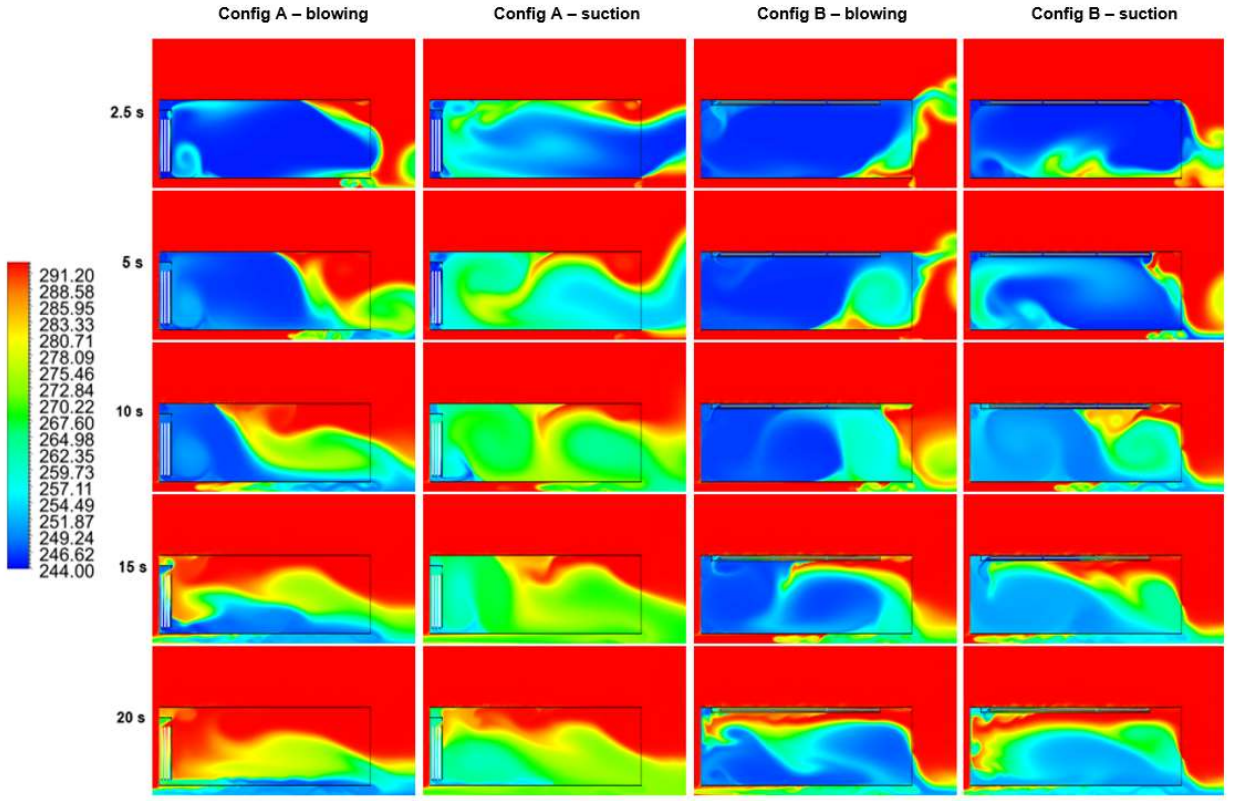

Figure 4: Time evolution of temperature contours (K) for Configuration A – blowing and suction and Configuration B – blowing and suction at $t = 2.5$ s, 5 s, 10 s, 15 s and 20 s.

At $t = 2.5$ s, it is apparent from Figure 4 that the flow is dominated by the pre-existing flow inside the trailer. Some atmospheric air has been dragged into the trailer by the pre-existing flow through the top or bottom region of the trailer depending on the rotation of the pre-existing flow. As infiltration occurs at high velocity, as seen from Table 2 and Figure 3, peak infiltration occurs during this time interval. However, it is apparent from Figures 3 and 4, that the further infiltration and the penetration of hot atmospheric air is being prevented by the exiting flow near the doorway acting similar to an air curtain seen from Foster et al. (2006), Hayes and Stoecker (1969), and Tso et al. (2002).

At $t = 5$ s, hot atmospheric air begins to infiltrate and penetrate through the top region of the doorway. Flow inside the trailer is still being dominated by the pre-existing flow and its interaction with the incoming hot atmospheric air. Mixing of hot and cold air is very prominent near the doorway due to this interaction. From $t = 10$ s, further advancement of the hot atmospheric air into the trailer can be seen. However, circulation zones created by the pre-

existing flow and the initial hot atmospheric air that has been dragged into the trailer are now preventing further advancement of the hot atmospheric air into the trailer. This effect can even be observed until $t = 15$ s.

At $t = 20$ s, the hot air infiltration has reached the back of the trailer as the circulation zones have diminished. At this time, the influence of the pre-existing flow has vanished, and the flow is mostly due to the buoyancy effect. The infiltration rate profile from Figure 3, supports this statement as the infiltration rate is steady until $t = 35$ s. From $t = 35$ s, infiltration rate decreases slightly as the trailer is now filled with hot atmospheric air and the infiltration rate is being caused solely by the plates.

For both configurations, the mode of operation for the pre-existing flow can be seen to have a minor effect on the infiltration rate and the advancement of the atmospheric air into the trailer. The blowing mode takes 11.5% and 13.1% more time to reach the renewal time compared to the suction mode for Configurations A and B, respectively.

However, significant differences between Configurations A and B can be seen both from the temperature contours and the time evolution of the infiltration rate. Configuration B takes 91.0% and 88.5% longer to reach the renewal time compared to Configuration A for blowing and suction mode, respectively. The main reason for this can be inferred from the temperature contours in Figure 4 between $t = 0$ s to $t = 15$ s. For Configuration A in both operating modes, warm air infiltrates near the top region of the door at $t = 5$ s. However, in Configuration B, hot air infiltration is prevented by the exiting flow and the presence of the cold air near the plates. This effect is more prominently displayed at $t = 10$ s. For the blowing mode, cold air from the plates and the deflected exit of the pre-existing flow from the bottom-center of the trailer to the top can be seen preventing the infiltration of atmospheric air at the top of the doorway. For the suction mode, incoming atmospheric air at the top is blocked by the cold air surrounding the plates. It should also be noted that due to the presence of the plates, the path for the flow has also been narrowed. This causes further "blocking" of the infiltration of hot atmospheric air through the top.

3.3. Cargo

For the present case, 5 boxes full of frozen meat were considered. For Configuration A, the first box is located 0.2 m away from the separating wall and 0.15 m above the floor of the trailer to allow for the flow to pass through. Proceeding boxes are separated by 0.1 m from each other. The thermophysical properties of the cargo consisting of frozen meat and cardboard packaging were extracted from Paquette et al. (2017) and are shown in Table 3 with the thickness of the box mixed to be a standard value of 2 mm. The dimension of each box is fixed to be 1 m and 1.2 m in length and height respectively. Conduction through the boxes is incorporated into the simulations. The initial temperature of the cargo is set to be 258 K.

Table 3: Thermophysical properties of the cargo

Material	Density ρ ($kg.m^{-3}$)	Specific heat C_p ($J.kg^{-1}.K^{-1}$)	Thermal conductivity k ($W.m^{-1}.K^{-1}$)
Frozen meat	1050	3000	0.25
Cardboard packaging	276	1700	0.058

3.4. Steady State Results – Cargo

Identical to the transient simulations obtained from Section 3.2., steady state results are used as the initial conditions for the transient simulations. For the transient simulations with cargo, Configuration B – blowing was chosen for its better performance in terms of the renewal time. For Configuration A, suction mode was chosen for the comparison to be consistent with the direction of the rotation of the pre-existing flow within the trailer. Also, as seen from Section 3.2., Configuration A, blowing mode only performs slightly better with 11.5% increase in the renewal time compared to that of the suction mode.

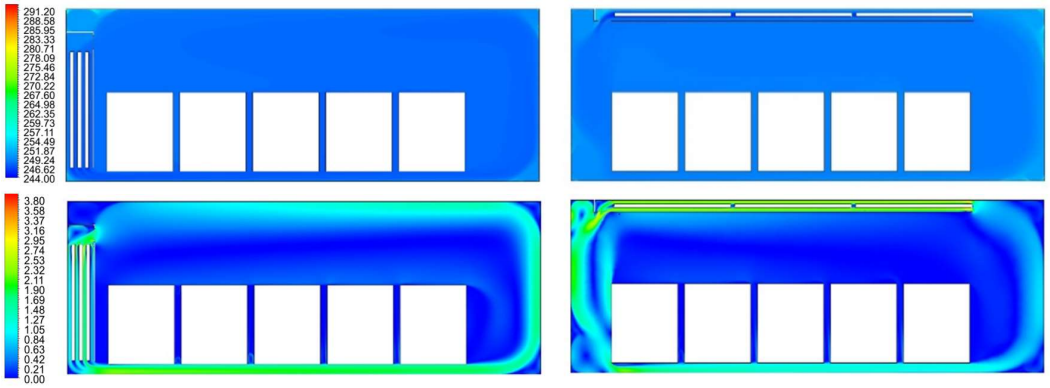

Figure 5: Temperature (K) and velocity ($m.s^{-1}$) contours for Configuration A with cargo (left) and Configuration B with cargo (right)

Even with the introduction of the cargo, it can be seen from Figure 5 that the temperature remains homogeneous throughout the trailer, with minor exceptions at the corners due to the presence of weak recirculation zones. The major difference is that in Configuration B, due to the presence of the cargo, the flow is being blocked by the narrow passage through the bottom and some of the flow is being deflected upwards. This generates a stronger recirculation zone at the back of the trailer. However, near the doorway, the flow structure remains relatively similar to the case without cargo in Section 3.1.

Table 4: Temperature and velocity data from the steady state simulations with cargo

Configuration	Area-averaged Temperature (K)	Area-averaged Velocity ($m.s^{-1}$)	Maximum Cargo Temperature (K)	Minimum Cargo Temperature (K)
A – suction	244.9	3.24	244.9	244.8
B – blowing	245.1	2.46	245.2	245.1

The initial area-averaged velocity for Configuration B is 31.7% lower than that of Configuration A due to the blockage of the flow seen at the location of the first cargo. For both configurations, the temperature inside the cargo is nearly homogenous with a minor difference of 0.1 K or less for Configurations A and B. However, it should be noted from Table 4 that there is a slight temperature difference of 0.3 K between the maximum cargo temperatures observed for Configurations A and B.

3.5. Transient Results – Cargo

Due to the introduction of the cargo, it can be seen from Table 5, that the renewal time for Configuration A increased by 96.2%. However, for Configuration B, the renewal time decreased by 8.3% with an increase of 71.0% in the peak infiltration rate.

Table 5: Infiltration data for Configurations A and B with cargo

Configuration	Renewal Time (s)	Peak infiltration rate ($m^3.s^{-1}$)	Peak infiltration time (s)
A – suction	13.0	10.5	0.7
A – suction – cargo	25.5	10.7	0.6
B – blowing	27.7	3.1	0.3
B – blowing – cargo	25.4	5.3	0.7

From Figure 6, it is apparent that after 20 seconds, Configurations A and B with cargo perform nearly identical to each other, corresponding to the identical obtained renewal times. Due to the cargo, the presence of the circulation zones inside the trailer from Section 3.2. cannot be seen. Whereas in the first few seconds, the pre-existing flow within the trailer near the doorway exits the trailer. The effect of this is more evident for Configuration A as the initial velocity inside the trailer is 31.7% higher than for Configuration B.

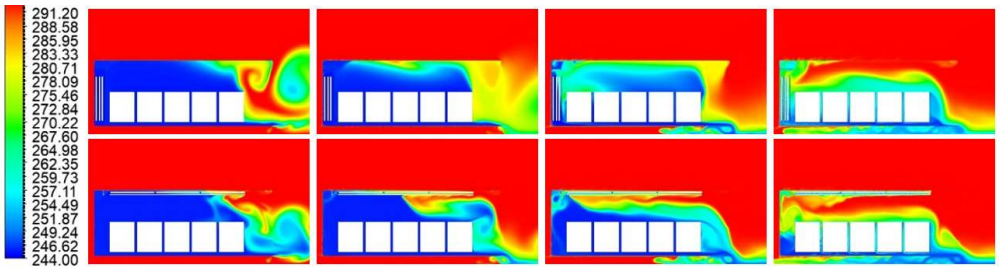

Figure 6: Temperature contours (K) at t = 2.5 s, 5 s, 10 s and 20 s (left to right) for Configurations A (top) and B (bot)

Between $t = 5$ to 10 s, the effect of the pre-existing flow diminishes, and the buoyancy effect begins to predominate. The atmospheric air begins to infiltrate through the top region of the trailer, but the exiting cold air through the top region of the cargo restricts the infiltration. This limited infiltration of the atmospheric air causes the increase in the renewal time for Configuration A with cargo. At $t = 20$ s, the flow is entirely driven by buoyancy while the effect of the pre-existing flow within the trailer cannot be observed.

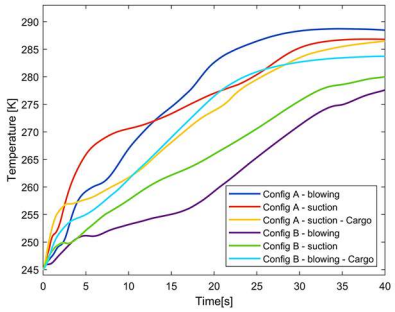

Figure 7: Time evolution of the area-averaged temperature inside the trailer

From Figure 3 b) and Figure 7, it can be observed that due to the higher pre-existing flow velocity for Configuration A, the infiltration of the atmospheric air is less pronounced than for Configuration B between $t = 5$ and 20 s. The exiting pre-existing flow strongly mixes with the atmospheric air, which delays the infiltration of pure atmospheric air. Therefore, the temperature inside the trailer also increases slower than in Configuration B, as supported by the lower temperature change observed in this time interval from Figure 7.

Table 6: Maximum temperature (K) of the cargo at $t = 40$ s

Configuration	Cargo 1	Cargo 2	Cargo 3	Cargo 4	Cargo 5
A	246.7	247.3	247.4	247.6	247.9
B	247.5	249.1	249.9	249.8	249.8

As the temperature change is higher for Configuration B after the pre-existing flow exits the trailer, the cargos inside the trailer are exposed to the atmospheric air quicker than those of Configuration A. Therefore, as shown in Table 6, the maximum temperature observed at each cargo after 40 seconds is also higher than that of Configuration A. The temperature difference is greater than that of the initial maximum-temperature difference of 0.3 K observed in Table 4. A maximum temperature difference of 2.5 K is observed for the Cargo 3 (middle) and a minimum temperature difference of 0.8 K is observed for the Cargo 1 (inner-most) between Configurations A and B, respectively. It should be noted that for Configuration B, the highest cargo temperature is observed at the Cargo 3 as the exiting cold air on top of the cargo and the recirculation zones at the back of the trailer mixing with the infiltrated atmospheric air delays other cargo boxes from making contact with the infiltrating high-temperature air. For Configuration A, the highest cargo temperature is observed at the Cargo 5, as the exiting cold air mixed with the atmospheric air makes the earliest contact and increases its temperature.

4. CONCLUSION

Former works of Croquer et al. (2019) and Bonaventure et al. (2020) were extended to optimize the configuration of the refrigeration system with the eutectic plates in terms of the trailer temperature and the cargo temperature by analyzing the air flow and the infiltration heat load into the refrigerated truck trailer during the door opening period. Without cargo, the configuration with the plates placed in series on the roof of the trailer noticeably improve the performance in terms of trailer temperature with respect to the configuration with the plates in series placed at the back of the trailer. However, introduction of the cargo into the simulation eliminates the effects of the circulation zones within the trailer that acts to prevent the infiltration of the atmospheric air. For the configuration with the plates placed on the roof of the trailer, due to the lower initial velocity of the pre-existing flow inside the trailer caused by the blockage of the flow by the cargo, atmospheric air was able to infiltrate and increase the temperature of the trailer earlier, resulting in a higher maximum temperature observed for the cargo. As the number of cargo boxes will progressively decrease during the entire delivery cycle, it is plausible that the configuration with the plates placed on the roof of the trailer could improve the performance as the influence of the pre-existing flow seen without the cargo will progressively emerge. The influence of the cargo parameters such as cargo locations, dimensions, arrangements, etc., should be investigated as it has a significant influence over the development of the pre-existing flow inside the trailer. Further developments should include a multiphase model to account for the humidity of air, phase change of the eutectic mixture and the formation of frost and ice along the plates.

REFERENCES

Azzouz, A., Gossé, J., & Duminil, M. (1993). Détermination expérimentale des pertes de froid occasionnées par l'ouverture d'une porte de chambre froide industrielle, *Revue Internationale du Froid, 16* (1), 57-66.

Bonaventure, M., Benchikh Le Hocine, A.E., Croquer, S., Huchtemann, K., & Poncet, S. (2020). Heat and mass transfer in a loaded truck trailer equipped with eutectic plates: a comparative numerical study. 6th IIR Conference on Sustainability and the Cold Chain, Nantes, France.

Croquer, S., Benchikh Le Hocine, A.E., & Poncet, S. (2019). Numerical modelling of heat and mass transfer in a refrigerated truck trailer. 25th IIR International Congress of Refrigeration, Montréal, Canada.

Foster, A. M., Swain, M. J., Barrett, R., & James, S. J. (2003). Experimental verification of analytical and CFD predictions of infiltration through cold store entrances. *International Journal of Refrigeration*, *26*(8), 918-925.

Foster, A. M., Swain, M. J., Barrett, R., D'Agaro, P., & James, S. J. (2006). Effectiveness and optimum jet velocity for a plane jet air curtain used to restrict cold room infiltration. *International Journal of Refrigeration*, *29*(5), 692-699.

Hayes, F. C., & Stoecker, W. F. (1969). Design data for air curtains. *Ashrae Transactions*, *75*(2), 168-180.

Hoang, M. L., Verboven, P., De Baerdemaeker, J., & Nicolaı, B. M. (2000). Analysis of the air flow in a cold store by means of computational fluid dynamics. *International Journal of Refrigeration*, *23*(2), 127-140.

Lafaye de Micheaux, T., Ducoulombier, M., Moureh, J., Sartre, V., & Bonjour, J. (2015). Experimental and numerical investigation of the infiltration heat load during the opening of a refrigerated truck body. *International Journal of Refrigeration*, *54*, 170-189.

Paquette, J. C., Mercier, S., Marcos, B., & Morasse, S. (2017). Modeling the thermal performance of a multilayer box for the transportation of perishable food. *Food and Bioproducts Processing*, *105*, 77-85.

Tassou, S. A., De-Lille, G., & Ge, Y. T. (2009). Food transport refrigeration–Approaches to reduce energy consumption and environmental impacts of road transport. *Applied Thermal Engineering*, *29*(8-9), 1467-1477.

Tso, C. P., Yu, S. C. M., Poh, H. J., & Jolly, P. G. (2002). Experimental study on the heat and mass transfer characteristics in a refrigerated truck. *International Journal of Refrigeration*, *25*(3), 340-350.

UN Economic Commission for Europe (2018). ATP as amended on 6 January 2018 – Agreement on the International Carriage of Perishable Foodstuff and on the Special Equipment to be used for such Carriage.

ACKNOWLEDGEMENTS

The authors would like to thank the NSERC chair on industrial energy efficiency established at Université de Sherbrooke in 2019 and supported by Hydro-Québec, Natural Resources Canada (CanmetEnergy in Varennes) and Emerson Commercial and Residential Solutions, particularly Juan Catano Montoya from Emerson Commercial and Residential Solutions for his support and involvement. Calculations have been performed using the supercomputer Béluga and Graham clusters of Compute Canada's network, which is also gratefully acknowledged.